Article

Application of Time Series INSAR (SBAS) Method Using Sentinel-1 for Monitoring Ground Deformation of the Aegina Island (Western Edge of Hellenic Volcanic Arc)

Ioanna-Efstathia Kalavrezou [1], **Ignacio Castro-Melgar** [1,2], **Dimitra Nika** [3], **Theodoros Gatsios** [1], **Spyros Lalechos** [4] **and Issaak Parcharidis** [1,*]

[1] Department of Geography, Harokopio University, 176 76 Athens, Greece; gs21779@hua.gr (I.-E.K.); icastromelgar@ig.cas.cz (I.C.-M.); gatsios@hua.gr (T.G.)
[2] Institute of Geophysics, Czech Academy of Sciences, 141 00 Prague, Czech Republic
[3] School of Rural, Surveying and Geoinformatics Engineering, National Technical University of Athens, 157 80 Athens, Greece; nikadimitragis@gmail.com
[4] Earthquake Planning & Protection Organization of Greece, 154 51 Athens, Greece; slalexos@oasp.gr
[*] Correspondence: parchar@hua.gr

Abstract: This study employs advanced synthetic aperture radar (SAR) techniques, specifically the small baseline subset (SBAS) method, to analyze ground deformation dynamics on Aegina, a volcanic island within the Hellenic Volcanic Arc. Using Sentinel-1 satellite data spanning January 2016 to May 2023, this research reveals different deformation behaviors. The towns of Aegina and Saint Marina portray regions of stability, contrasting with central areas exhibiting subsidence rates of up to 1 cm/year. The absence of deformation consistent with volcanic activity on Aegina Island aligns with geological records and limited seismic activity, attributing the observed subsidence processes to settlement phenomena from past volcanic events and regional geothermal activity. These findings reinforce the need for continuous monitoring of the volcanic islands located in the Hellenic Volcanic Arc, providing important insights for local risk management, and contributing to our broader understanding of geodynamic and volcanic processes.

Keywords: volcanic risk; ground deformation; SBAS method; Sentinel-1; Aegina Island; Hellenic Volcanic Arc

1. Introduction

In the context of Aegean Greek geography, the striking landscapes and island formations predominantly result from volcanic activity. The Hellenic Volcanic Arc has been active for approximately 4.7 Ma, continuing up to the current era [1,2]. Santorini, although the most prominent example, is just one among several active volcanic systems in this arc. This ongoing activity is evidenced by historical eruptions at various locations along the arc, including Methana, Milos, Santorini, Kolumbo, and Nisyros. This arc also includes other islands, such as Aegina and Poros, which were geologically shaped by the ongoing subduction of the African tectonic plate beneath the Eurasian plate [3]. Within this volcanic arc, Aegina Island represents one of the notable geologically active systems. Aegina is an island situated in the Saronikos Gulf, at a distance of 27 km from Athens, covering an area of approximately 87 km^2 (Figure 1). This island belongs to the Aegina-Poros-Methana volcanic fields. Aegina, along with other volcanic formations in the Saronikos Gulf, predominantly exhibits monogenetic characteristics, lacking any complex composite volcanic structures [2].

Saronikos Gulf hosts the northwestern end of the South Aegean Active Volcanic Arc resulting from the subduction of the African plate beneath the Aegean microplate and the rollback of the overriding microplate. The Saronikosc Gulf is bordered, to the north and the northeast, by the densely populated Attica Peninsula, and to the west by the NW coastline

of Peloponnese. The region is characterized by moderate seismicity, with the northern and western Gulf margins exhibiting high-magnitude historical and recent earthquakes, associated with the presently active NS extensional tectonic regime [4]. Shallow seismicity in the Saronikosc Gulf is attributed to the extensional stresses and the deformation of the upper crust, while deeper seismicity, at sub-crustal levels, is related to the subducting oceanic slab at depths of 100–170 km, beneath Corinth, the Saronikosc Gulf, and Attica [5,6]. More specifically, from historical records to the present, there has been very little seismic activity near Aegina Island. There are also a few possibly active nearby faults with a small seismic capacity [7].

The western volcanic fields of Aegina-Poros-Methana occur in the Saronikos Gulf in the form of graben, active since the Pliocene [8]. The initial volcanic phase in Aegina, occurring from approximately 4.7 to 4.3 Ma, was marked by shallow-marine eruption that led to the formation of pillow lavas and tuffs [1,9,10]. Following the initial volcanic activities in Aegina, a subsequent period between 3.9 and 3.0 million years ago marked a significant shift toward the extrusion of predominantly andesitic and dacitic lavas. This era was characterized by the construction of extensive lava domes and flows, primarily in terrestrial settings [2]. The volcanic activity then entered a lull, only to be restarted around 2.1 to 2.0 Ma ago [2]. This later phase was distinguished by the eruption of lava, with compositions varying from andesitic to basaltic–andesitic, predominantly on land [3]. Paleomagnetical studies revealed that Aegina's most recent volcanic episodes correspond with the Matuyama polarity epoch during the Pleistocene period, and there has been an absence of notable volcanic activity on the island for the past 720,000 years [11]. While volcanism activity on Aegina subsided toward the end of the Pleistocene, currently, the region still exhibits a geothermal field of low temperature, indicative of the enduring geodynamic processes beneath the surface [12,13].
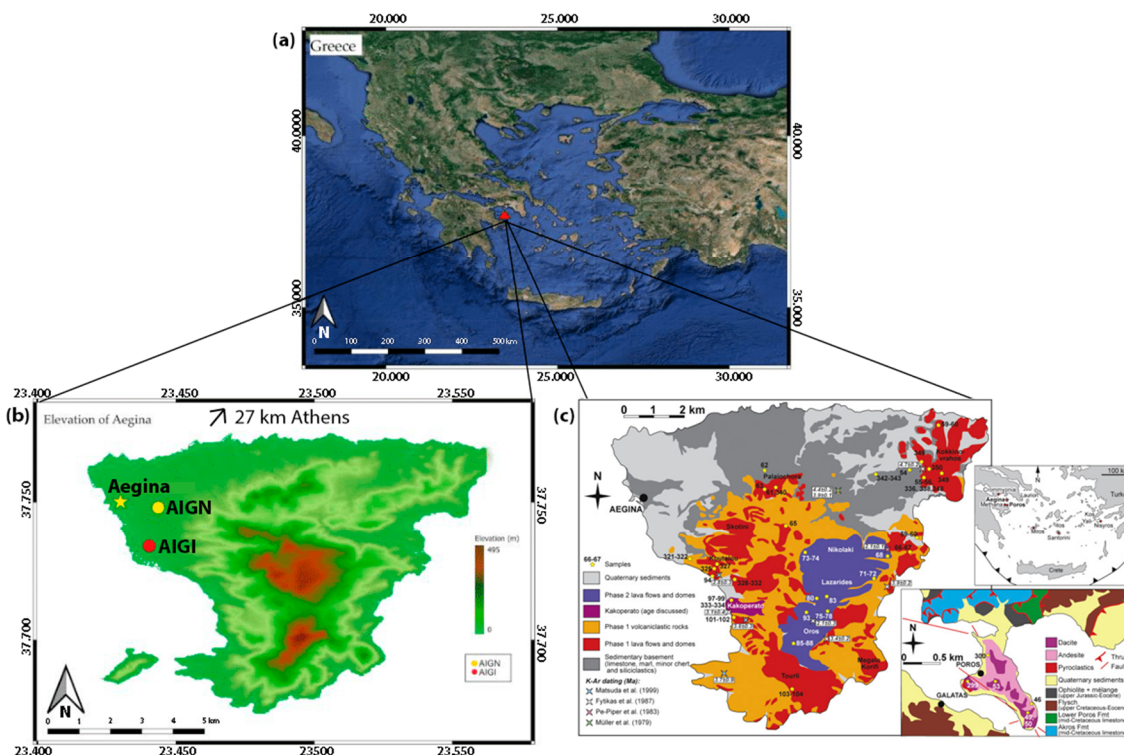

Figure 1. (**a**) Map of Greece. (**b**) Elevation map of Aegina. The yellow star shows the location of the town of Aegina, the yellow circle represents the AIGN seismic station, and the red circle the AIGI GNSS station. (**c**) Geological map of Aegina. Adapted with permission from Ref. [14]. 2024, Elsevier.

In the Western area of the Hellenic Volcanic Arc, such as Aegina or Methana, the volcanic risk is generally assessed as low based on the time of the last eruptions [15].

Nonetheless, various geological factors underscore the importance of detailed research into Aegina's volcanic system. The neotectonic structure of the Saronikosc Gulf, in which Aegina is situated, is identified as a zone of significant seismic activity [6]. These geological characteristics necessitate ongoing vigilance and study due to their implications for volcanic activity in the region. The Greek Institute of Geodynamics of the National Observatory of Athens (NOA) displayed one seismological station (Station AIGN) of the National Seismic Network (NOA HL) on Aegina Island [16]. Moreover, considering the risk factors, this volcanic island is in close proximity to Athens, located just under 27 km away. Should there be any resurgence in volcanic activity, it could have significant implications for Aegina's local community. The island typically hosts around 13,000 residents year-round, a number that rises notably during the summer months owing to its popularity as a tourist destination.

The goal of the current research is to analyze and detail the surface ground movements of the Aegean islands. This analysis is conducted through an advanced multi-interferogram approach, using synthetic aperture radar (SAR) data. The SAR images, provided by the Sentinel-1 satellites of the Copernicus Program, cover a period from 11 January 2016 to 22 May 2023. This study focuses on extracting and interpreting the relevant geophysical data from these satellite observations to gain a deeper understanding of the volcanic island's surface dynamics during this period.

The use of Interferometric SAR (InSAR) techniques has been extensively applied for the analysis and monitoring of surface deformation in various locations along the volcanic arc [17–25]. These applications have demonstrated the capability of InSAR to provide detailed, spatially comprehensive insights into volcanic activities [26,27]. Such activities include those related to the processes within magma chambers, as well as surface-level changes linked to hydrothermal activities, such as low-temperature venting [28,29]. Other recent uses of Persistent Scatterer InSAR (PS-InSAR) are land subsidence/uplift mapping [30,31]. However, despite the widespread application of InSAR in volcanic areas and its proven effectiveness, there appears to be a gap in the literature concerning its application to Aegina Island.

In consideration of Aegina's diverse landscape and vegetative cover, our study employed a Multi-Temporal InSAR (MT-InSAR) approach using the small baseline subset (SBAS) technique [32,33]. This method was specifically chosen to enhance our monitoring capabilities and to increase the number of measurable sites across the island [34]. The primary objective was to comprehensively analyze the geodynamic behavior of Aegina, with a particular focus on understanding surface deformation.

The assessment of volcanic risk on Aegina Island, as part of our study, carries significant practical implications, especially for the local community. By analyzing ground deformation patterns through advanced SAR techniques, our research provides critical insights into the current state of the volcanic activity on the island. These findings are pivotal in informing local authorities and disaster management institutions, aiding them in developing more effective risk management strategies. Specifically, the ability to predict potential areas of heightened risk can lead to timely evacuation plans and infrastructure reinforcement. Additionally, understanding the patterns of volcanic activity could contribute to long-term urban planning and emergency preparedness programs, ensuring that the local population is better protected against unforeseen volcanic events. Thus, this study not only advances scientific understanding but also serves a crucial role in enhancing the safety and resilience of the Aegina community against volcanic hazards.

2. Materials and Methods

There are many ways to use the satellite images and represent the land deformation. The data for this study were obtained from open-access sources, such as the Alaska Satellite Facility (ASF) of NASA. There is a large amount of data due to satellite images from the satellite platforms that use optical sensors or in neighboring bands. A SAR sensor operates in the microwave domain of the electromagnetic spectrum and has the ability to pass through weather factors, such as clouds, fog, and dust, making it a unique active system for

monitoring [35]. Another ability that increases the value of this radar system is its coherent sensor, which means it records both amplitude and phase information for each ground target [36–38].

The radar image (Figure 2) based on geometry has the coordinates of range and azimuth. The azimuth direction is parallel to the orbit of the satellite, while the range direction corresponds to the orthogonal line-of-sight (LOS) direction on the terrain of the radar's antenna. The phase and amplitude components both contribute to interpreting backscatter in SAR imagery. Amplitude values primarily represent the strength of the backscattered radar signal, indicating the energy returned from the ground surface or objects. The phase component indirectly provides information about the distance between the sensor and the target, aiding in timing and phase-shift analysis, and contributing to understanding target characteristics and geometry. According to the authors of [35,37,39], concerning the definition of the orbit that was used, the ascending orbit is when the satellite views the target area oriented eastward (moving from south to north). The use of SAR in deformation monitoring has been widely applied, and among the most used objectives is the monitoring of volcanic hazards [40,41], analysis of large earthquakes [42,43], subsidence related to geothermal fields [44,45], and many others.
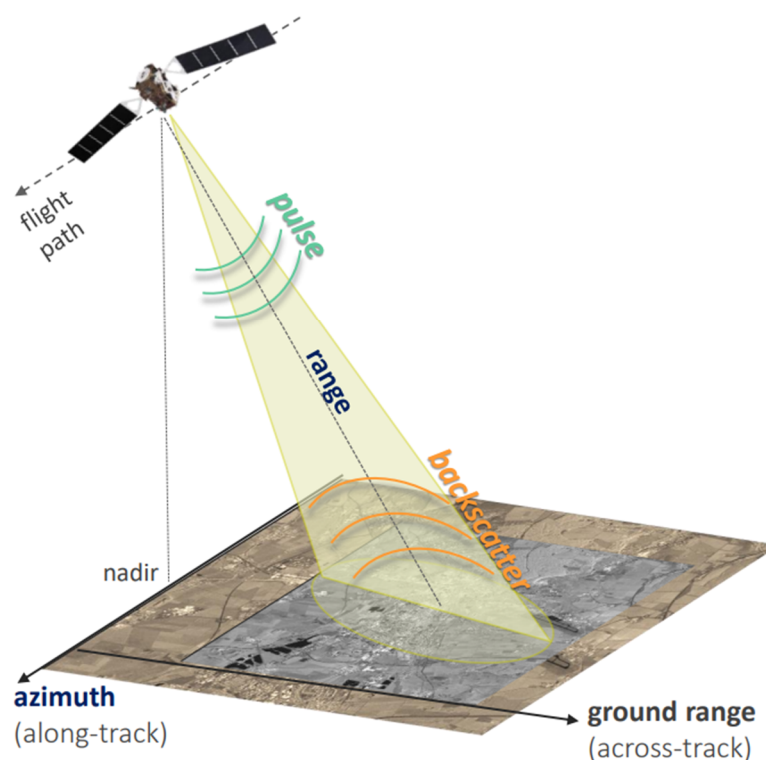

Figure 2. Scheme of synthetic aperture radar (SAR) acquisition. Adapted from [45].

In this work, the data that were acquired to be used were 171 single-look-complex (SLC) images taken by the Sentinel-1 satellite in interferometric wide (IW) mode from the ascending orbit. The SLC scenes span the period from January 2016 to May 2023. Sentinel-1 is part of the European Space Agency's Copernicus Program. It was designed for Earth observation, and it offers a comprehensive overview of the mission's goals, details about the satellite, and information about the ground segment [46,47]. These SLC images were processed using GAMMA RS (GAMMA Remote Sensing AG, Gümligen, Switzerland), Python, and bash scripting (Figure 3).
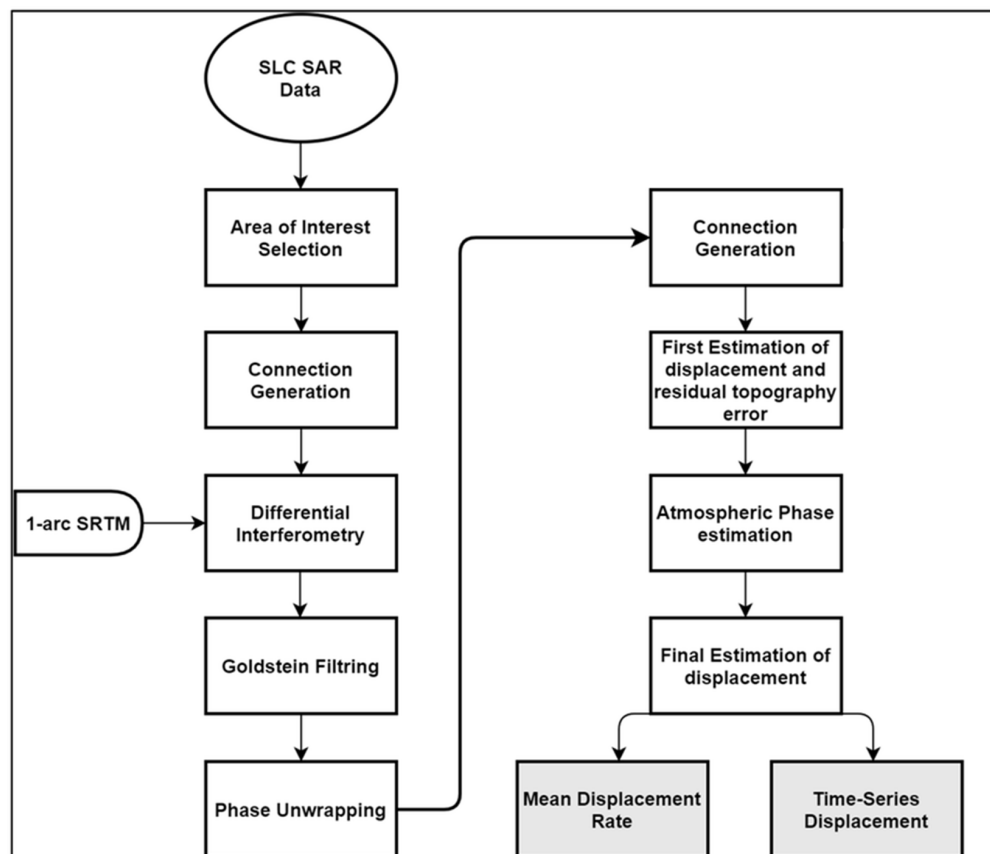
Figure 3. Flowchart of small baseline subset (SBAS) in GAMMA Remote Sensing v5.7 software. Adapted from [48].

The processing can be divided into two parts: pre-processing and the main processing. The first step of pre-processing was to update the orbital data of the SLC acquisition and to produce a big stack of 171 multi-look-images (MLI) in order to reduce the noise (speckle). Afterward, those MLI images were co-registered to a master image (4 September 2019) that had been carefully selected in the middle of the period of study and without adverse weather conditions for successful results. This co-registered stack was georeferenced using the SRTM-1 arcsec digital elevation model (DEM). The main process was carried out using the small baseline subset (SBAS) method. This method was chosen for monitoring surface deformation due to its millimeter-level precision because of its ability to overcome spatial and temporal decorrelation [49]. The GAMMA packages that were used for the pre-processing were the Modular SAR Processor (MSP), the Differential Interferometry/Geocoding (DIFF/GEO) package, the Interferometric SAR Processor (ISP), and the Land Applications Tools (LAT). During SBAS processing, the average-intensity image was created based on all the MLI images, and multi-reference stack pairs were determined using a maximum perpendicular baseline of 233.1 m (Figure 4). The next step was the generation of the interferograms between the pairs and the application of a spectral filter to smooth the phase in areas with intermediate to high coherence. The differential interferograms were unwrapped spatially, and later the linear ramps were estimated and removed. Then, the atmospheric phase component was estimated and subtracted. A standard deviation filter was applied to mask the low-quality part of the phase, and later the remaining phase was converted to displacement, producing deformation maps [50–53]. During the SBAS processing, the DIFF/GEO and ISP packages were used again, as well as the Interferometric Point Target Analysis (IPTA) and the Display Tools and Utilities (DISP) of GAMMA.
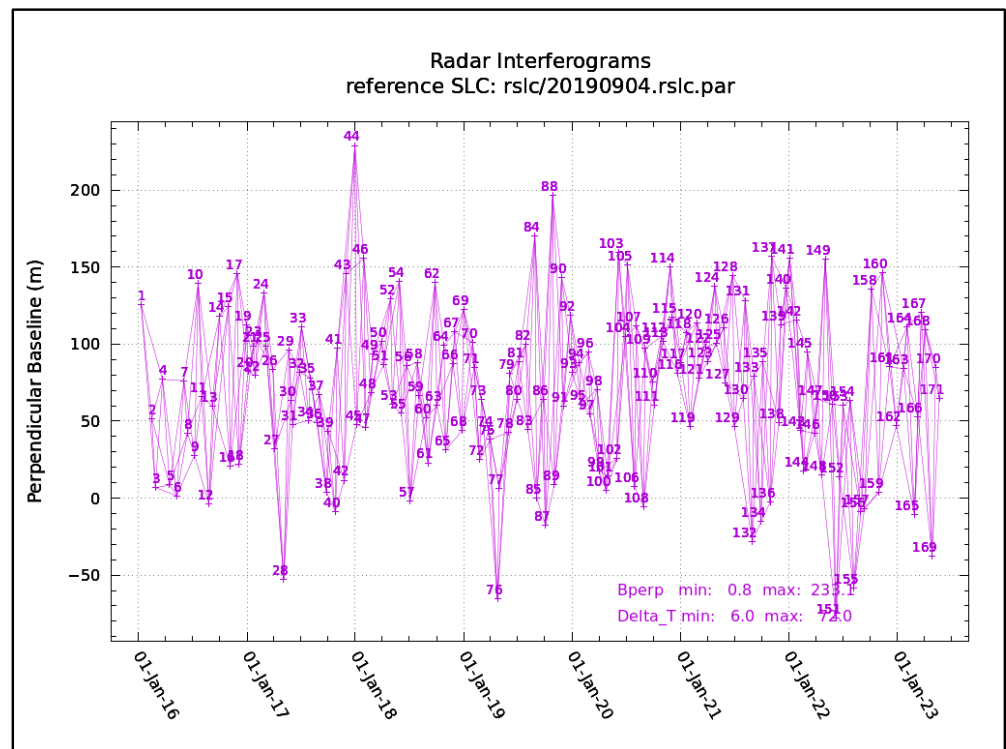
Figure 4. Plot between perpendicular baseline and date. Each line represents an interferometric pair used for the SBAS.

Interferometric coherence serves as a common gauge for assessing the quality of the interferometric phase in remote sensing applications. It is defined as the normalized cross-correlation between two SAR images that have been co-registered. Ranging between 0 and 1, the absolute value of coherence indicates the degree of similarity between the images. When all backscattering elements maintain their relative position and scattering strength over time, coherence tends to be high, as observed in bare soil and urban areas. Conversely, if elements shift or alter their microwave signature, coherence diminishes, often seen in vegetated surfaces with high fractional canopy cover and water bodies [54]. The island of Aegina is characterized by being a typical Mediterranean island: there are arid soils, bushes, pines, and different types of agriculture adapted to the dry conditions that characterize the island, such as olive trees, pistachio trees, or vines [55]. This makes the use of InSAR techniques very appropriate in this territory because the presence of these soils favors high coherence in the analysis.

The coherence map for the island of Aegina is presented in Figure 5. In general, it is considered that for a coherence value of less than 0.2, the results are not reliable enough [56,57]. To guarantee confidence in the obtained results, a mask with a value equal to or greater than 0.3 was applied (Figure 6). The regions in white are considered to have a sufficient coherence value (equal to or greater than 0.3) to be considered in the discussion.

The Global Navigation Satellite System (GNSS) data from the AIGI station (Figure 1) belonging to the Uranus network were used to validate the InSAR measurements. The data were converted into the InSAR line-of-sight vector using the InSAR imaging geometry for the ascending relative orbit 102. The observed velocities (V_E, V_N, and V_U, along the east–west, north–south, and vertical directions, respectively) and the associated errors from AIGI station in 2015 and between 2022 and 2023 are presented in Table 1.
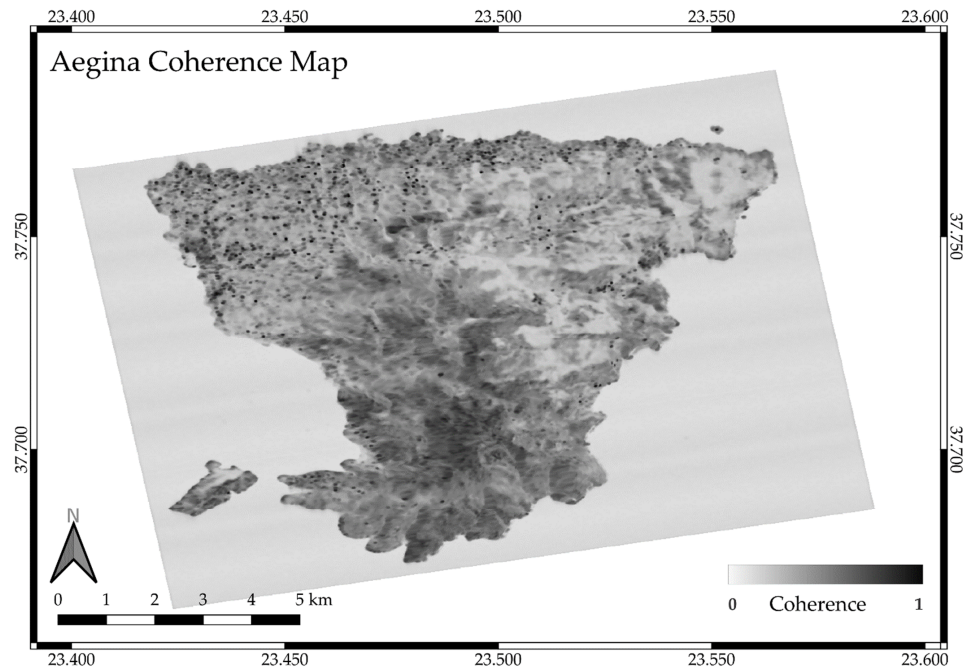
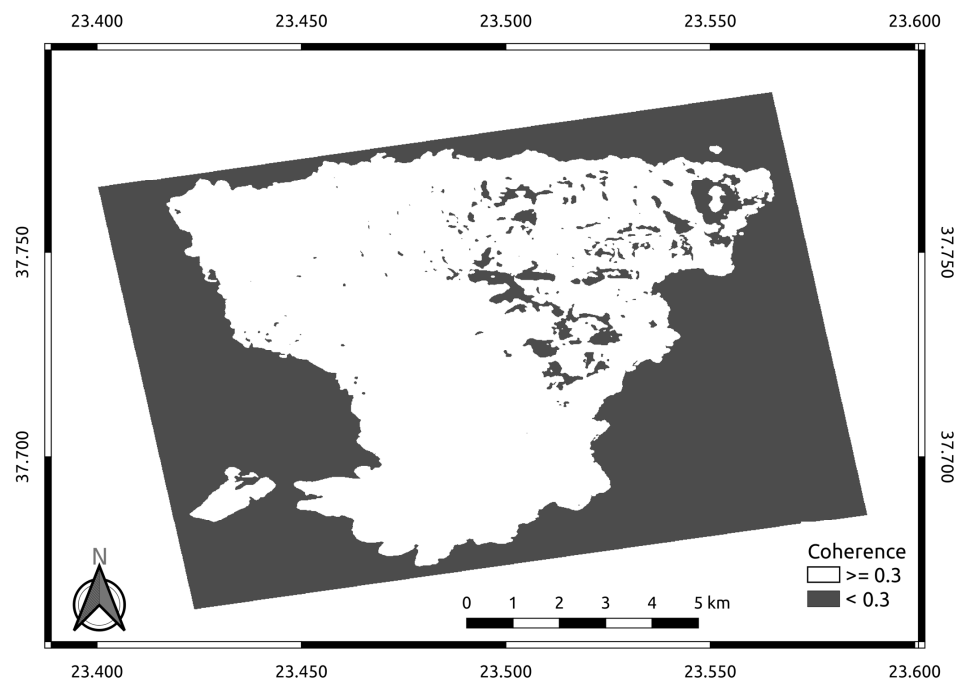**Figure 5.** Coherence map for the study area. The regions with the best coherence are presented in black.

Figure 6. Areas with coherence equal to or greater than 0.3 are shown in white, while areas in black show coherence of less than 0.3.

Table 1. Velocity values and the associated errors of the AIGI GNSS station on Aegina Island in the IGb14 reference frame. Notations: V, velocity; E, east–west; N, north–south; U, vertical/up.

Station	V_E (mm/year)	V_N (mm/year)	V_U (mm/year)
AIGI	9.04 ± 0.08	-11.70 ± 0.16	2.98 ± 0.32

3. Results

In this study, the SBAS technique was used to process Sentinel-1 data from January 2016 to May 2023. The monitoring results are shown in Figure 7. The first image refers to the cumulative deformation rate between the dates of this study, while the second image refers to the deformation rate.
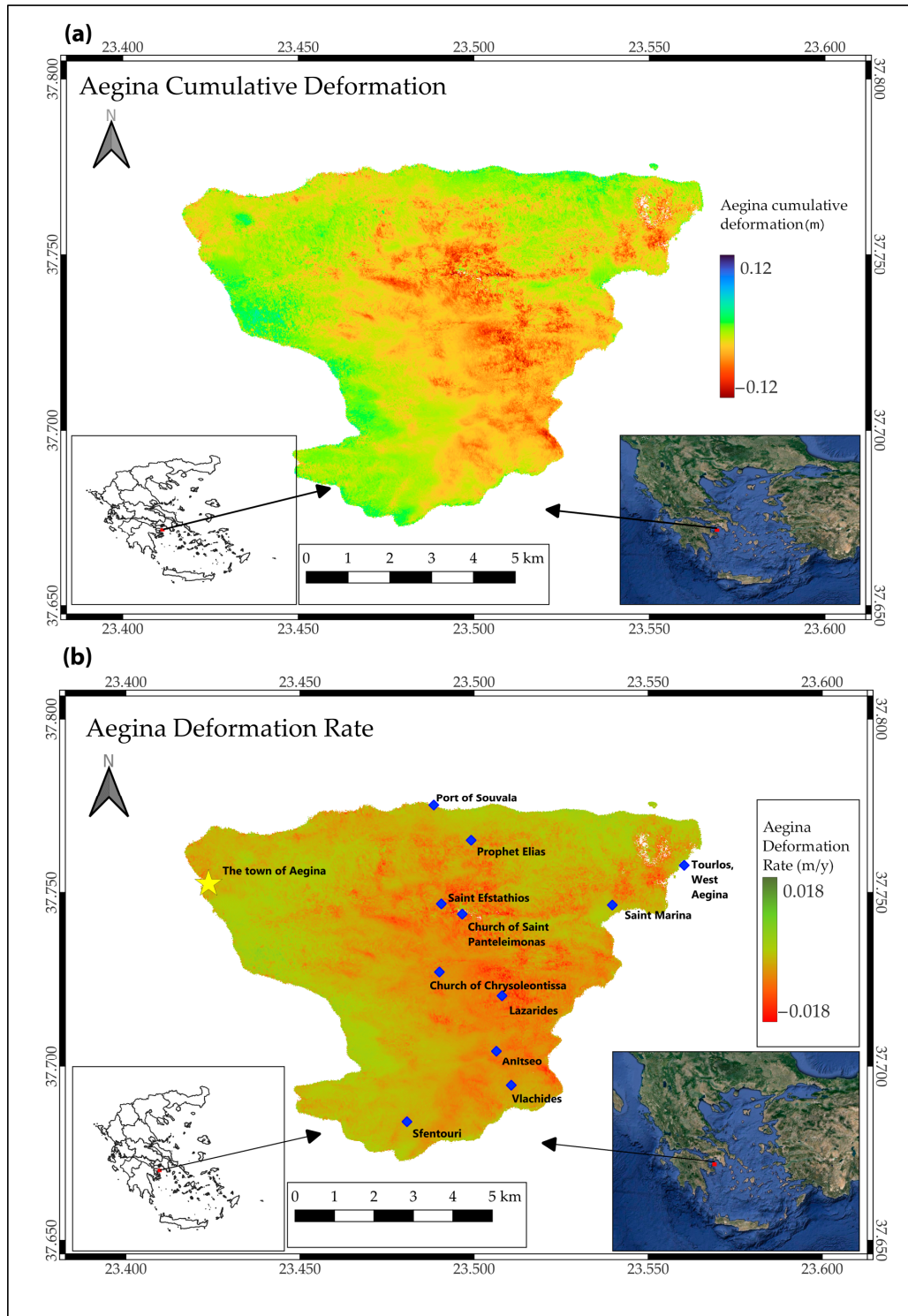

Figure 7. (**a**) Aegina Island cumulative deformation from January 2016 to May 2023. (**b**) Aegina Island deformation rate with marks from January 2016 to May 2023.

The monitoring results showed that various degrees of uneven land subsidence occurred on Aegina Island between 2016 and 2023. These areas are concentrated in the central part of the island, to the southeast and northeast. In these regions, a deformation of up to −0.12 m was reached. On the other hand, it can be seen how the western and northern areas showed a predominance of stability.

To provide a more detailed description of the spatial and temporal pattern of land subsidence on Aegina Island, we selected 12 points of interest throughout the island to analyze these variables in detail (Figures 8 and 9).
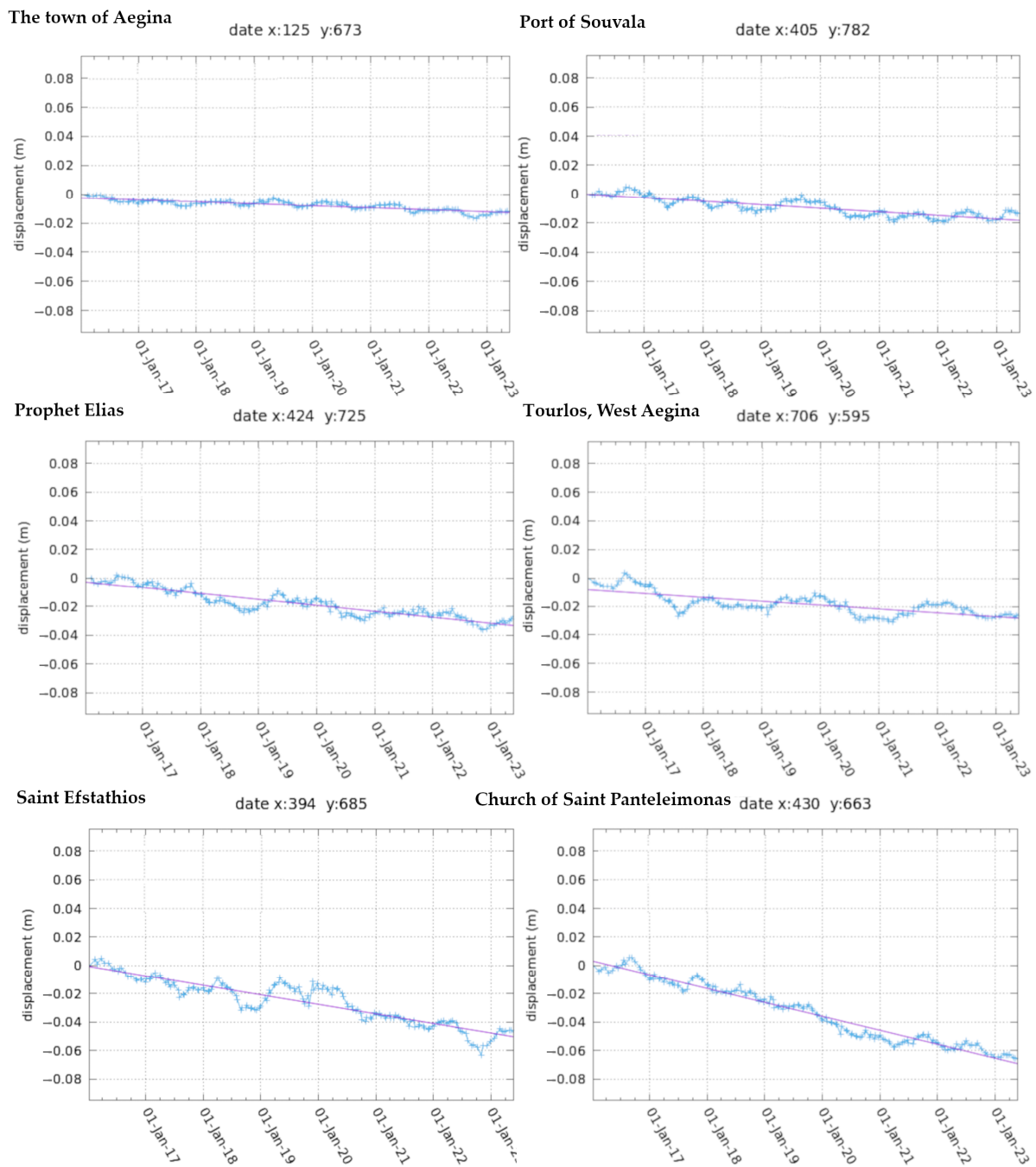

Figure 8. Temporal analysis of land deformation for the town of Aegina, Port of Souvala, Prophet Elias, Tourlos (West Aegina), Saint Efstathios, and Church of Saint Panteleimonas.
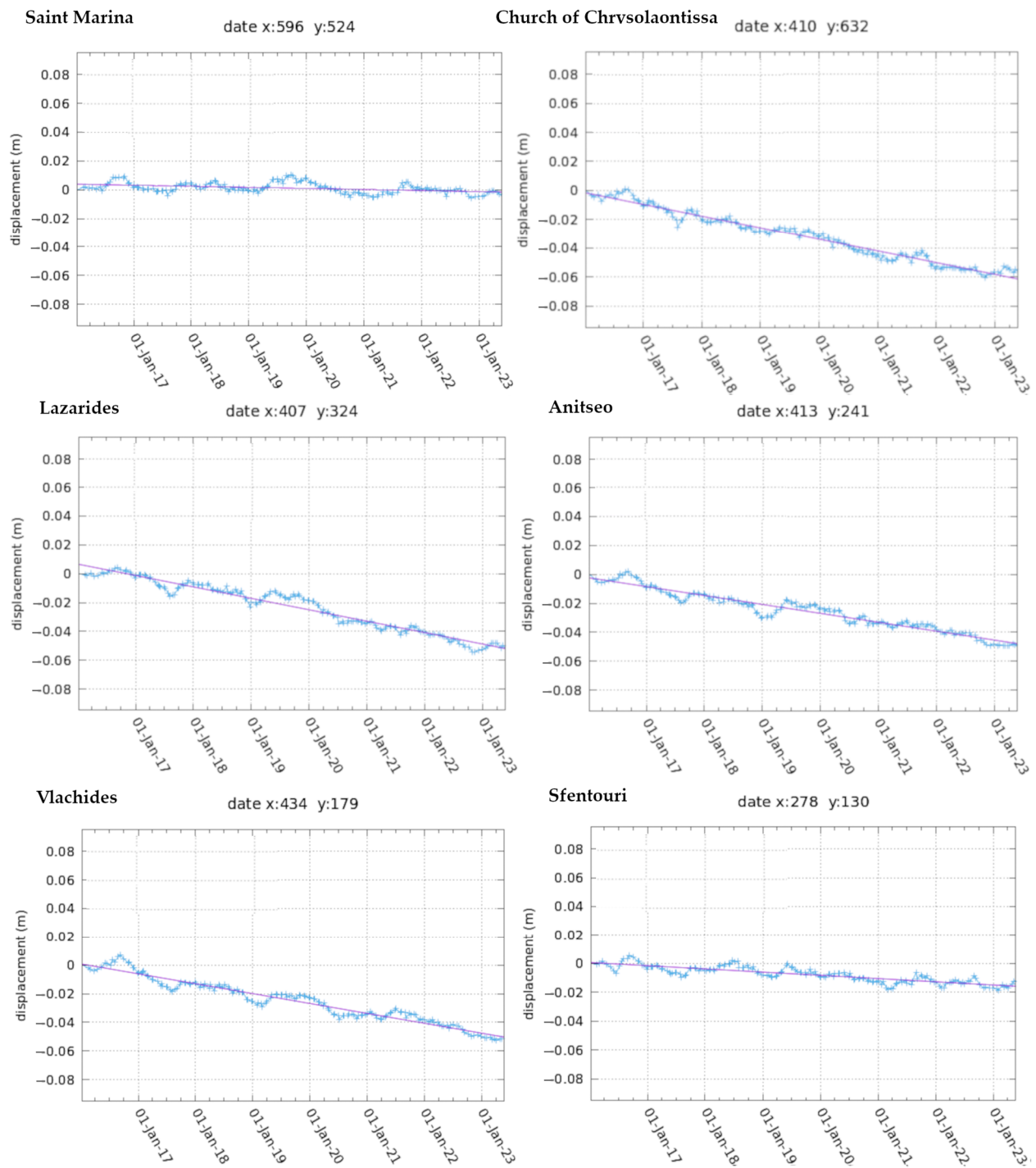
Figure 9. Temporal analysis of land deformation for Saint Marina, Church of Chrysoleontissa, Lazarides, Anitseo, Vlachides, and Sfentouri.

Figure 8 shows the temporal graphs of the evolution of deformation at six points of interest in the northern area of the island. The town of Aegina is the capital of the island and the population with the most inhabitants (around 7000), which makes it one of the most relevant study points. It is located in the northwestern area of the island in an area of relative stability. Observing the temporal graph, it is possible to appreciate the same stability that the deformation and accumulated deformation graphs show for the entire island. In the 7 years and 5 months of study, a cumulative subsidence of 1 cm can be observed. The Port of Souvala represents the northernmost point of interest on the island studied. The

northern area of the island has been observed as stable according to the work carried out, a trend that is corroborated in the time graph. The total displacement in the period studied was −0.02 m. Southeast of the Port of Souvala, but still in the northern part of the island, is Prophet Elias, a transition region between the more stable northern area and the central area, with higher subsidence values. This time graph shows how a subsidence of close to 4 cm accumulated over 7 years and 5 months. Continuing in the northern part of the island, focusing on the eastern part is Tourios, where there was an accumulation of about 3 cm at the time of study. Saint Efstathios and the Church of Saint Panteleimonas are located in the central area of the island, and in this region, the highest values of subsidence accumulated. Firstly, Saint Efstathios showed a total deformation of the terrain that reached 5 cm in the almost seven-and-a-half-year period. During this time, subsidence did not always maintain a constant rhythm, reaching periods of lower rhythm, as in 2019, or of a greater depth in these changes, as in the second half of 2022. In this year, the displacement reached figures greater than 6 cm, although as can be seen in the graph, there was a subsiding trend that deserves to be studied. In the case of the Church of Saint Panteleimonas, the accumulation of subsidence was even greater, reaching 7 cm, which indicates that in this case, there is an approximate deformation ratio of 1 cm/year. The variability of the ground deformation in this case was more stable than in the previous point.

The following temporal graphs to be delved into are found in points located mainly in the central and southern regions of the island of Aegina (Figure 9), with the exception of the town of Saint Marina in the northeast area. Agia Marina (Saint Marina) is the main town in the eastern part of the island and an attractive tourist region in the summer. It is located in a stable region, as corroborated by the temporal graph, where hardly any changes were seen. The Church of Chrysoleontissa and Lazarides are located in the central part of the island, a more unstable region. In the first case, the Church of Chrysoleontissa accumulated a stable subsidence of close to 1 cm/year (more than 6 cm in the period studied), with hardly any changes in the ratio. At the second point considered, Lazarides, the subsidence was less pronounced than the previous one, although it still accumulated 5 cm in the more than 7 years considered. Anitseo is located in the southern part of the island in a transition area between higher deformation ratios, such as those seen at Lazarides or the Church of Chrysoleontissa, and more stable areas to the south and southwest. Anitseo maintained a stable negative deformation in the study period, reaching 5 cm of subsidence in 7 years and 5 months. The same number was reached by Vlachides further south of Anitseo, and in both cases the deformation rate was mainly stable over the years, with small fluctuations visible in both points considered. The last point of interest considered for this study was Sfentouri—it is the southernmost point of the island, in the southwestern area. As can be seen in Figure 7, a mainly stable temporal graph could be expected for this point, a fact that was corroborated by reaching less than −0.02 m of displacement in the period studied between 2017 and 2022.

As can be seen in Figures 7–9, there are different zones of terrain deformation on the island of Aegina. In regions that are mainly located to the north and west of the island, the deformation behavior found in our study was stable. In these regions, the town of Aegina, the Port of Souvala, or the town of Saint Marina can be highlighted. There are other areas, mainly in the north and east of the island, where there was a subsidence process, as confirmed by the temporal graphs of the present study. These maxima, reaching approximately 1 cm/year, are found in the central part of the island. It is in this region that the churches of Saint Panteleimonas, Saint Efstathios, Chrysoleontissa, or Lazarides predominate.

4. Discussion

The SBAS technique is a fundamental tool for monitoring deformations. In the case of this study, the climatic conditions and the type of soil of the Aegean Islands [51] favored high coherence that allowed for highly reliable results. The analysis of Figure 5 allowed to find small areas in the east and center of the island with poor coherence that did not

allow for analysis. These regions correspond to those areas with the greatest forest presence on the island. Despite encountering these areas with low coherence in the InSAR results, the overall findings remained robust. This is because the coherent regions, where the data were reliable, consistently demonstrated the same subsidence trend. Therefore, while small pockets of low coherence may exist, they did not significantly impact the overall interpretation of the results, as the coherent areas provided a reliable representation of the subsidence pattern. Although the data showed high reliability, InSAR deformation studies can be improved in future work with the use of different orbits to improve the accuracy of deriving LOS deformation. The LOS velocity in AIGI station was estimated at −0.004 m/year. This result agrees with the InSAR results of this study.

The application of GAMMA Remote Sensing v5.7 software, in conjunction with the SBAS technique, proved to be highly sensitive to displacement detection, showcasing its efficacy in capturing ground deformation patterns. The results obtained from the Sentinel-1 data spanning from January 2016 to May 2023 revealed a discernible sedimentation trend on Aegina Island. The utilization of time series analysis elucidated both steady and unsteady ground relocations, providing valuable insights into the complex geodynamic activity in the region.

The inclusion of a strategically chosen stationary point (reference point) within the town of Aegina, situated at a distance from the sea and forests, enhanced the reliability of the acquired relocation rates. This point, selected for its potential impact on the overall results, played a crucial role in achieving a comprehensive understanding of the deformation dynamics on the island.

The region of the western edge of the Hellenic Volcanic Arc showed signs of geodynamic activity that must be monitored by different techniques, including different indicators. In the case of deformation, the results of the present study showed an island with two regions that showed different behaviors: a stable region in the western and northern parts of the island, and a region in the east and central parts with subsidence processes. The correlation between deformation rates observed in Aegina and the corresponding time series data, coupled with geological considerations, underscores the presence of ground displacement over the study period. Notably, the towns of Aegina, Saint Marina, Sfentouri, Souvala, and Tourlos exhibited low cumulative displacement ranging from 0 to −0.02 m in the period of study and, therefore, these areas are considered stable. In contrast, points including Prophet Elia, Saint Efstathios, Church of Chrysoleontissa, Church of Saint Panteleimonas, Lazarides, Anitseo, and Vlachides manifested higher displacement rates (deformation ratios of around 1 cm/year). The geological map of Aegina (Figure 1c) aligned with these findings, attributing the variations in displacement to volcanic occurrences.

The cumulative deformation map, as illustrated in Figure 7, stands as a depiction of Aegina's ground displacement throughout the study duration. The corresponding time series data extracted from this map provided further insights into the intricate dynamics of the observed changes. For displacement values across the island, the discernible connection with the presence of lava domes and flows on the ground underscores the profound geological influence in shaping the observed ground deformation. It became evident that areas exhibiting higher ground displacement corresponded spatially with geological features, such as lava flows and domes (Figure 1c). This correlation underscores the intricate relationship between geological characteristics and ground deformation, suggesting that the geological composition plays a pivotal role in influencing the observed patterns of displacement. Quaternary sediments contributed to the stability observed at five points, including Sfentouri, even though it is situated in an area with volcaniclastic rocks, and Tourlos, despite being close to lava flows and domes. The geological features, particularly lava flows and domes (phases 1 and 2) and volcaniclastic rocks, characterize the geological composition of the seven points exhibiting notable displacement from satellite observations.

Methana Peninsula and Poros Island are near Aegina and belong to the western edge of the Hellenic Volcanic Arc, located 7 and 12 km southwest and south of Aegina, respectively (Figure 1c). In Methana, there is a low volcanic risk, and it is seismically active with the

presence of geothermal activity. The results of Gatsios et al. [23], based on InSAR and GNSS, showed a ground deformation between −0.018 and 0.007 m/year. This work showed how the western part of the island demonstrated stability in deformation, while certain regions of the eastern part of the island showed subsidence processes due to geothermal processes and mass movements on the eastern flank of the volcano. These authors also presented data for Poros through a GNSS station, showing a moderate displacement, indicating stability in the region. The results obtained for these two areas are consistent with the results shown for the island of Aegina, as they are located in this region of the Hellenic Volcanic Arc. Using InSAR and GNSS, it was shown how these regions remained stable, except for regions with subsidence, where different geodynamic processes were mainly linked to geothermal activity and displacement of sedimentary masses.

The results showed that currently, the island of Aegina does not suffer deformation processes consistent with a future volcanic eruption in the short term. This fact is reinforced considering the time of the last volcanic event (0.72 Ma [1,2]), the type of volcanic activity (monogenetic field [2]), and the limited seismic activity with a hypocenter on the island [7,58]. However, the subsidence processes observed on the island are related to geodynamic activity concerning settlement processes of products from former eruptions and geothermal activity in the region [1,9,10,59]. This region has subsidence with rates of up to 1 cm/year.

5. Conclusions

Through the application of the SBAS technique, along with GAMMA Remote Sensing v5.7 software, in the period from January 2016 to May 2023, this study has provided valuable insights into the geodynamic activity and ground deformation patterns on the island of Aegina. This work is a pioneering study in monitoring deformation through InSAR analysis on this island.

The favorable climatic conditions and soil characteristics of the Aegean Islands facilitated high coherence in the results, enabling reliable detection of ground displacements. Despite encountering areas with low coherence, particularly in forested regions in the center of the island, the overall robustness of the findings remained intact. The coherent regions consistently exhibited a discernible subsidence trend, underscoring the reliability of the observed deformation patterns.

The delineation of distinct regions exhibiting different deformation behaviors highlights the importance of ongoing monitoring, particularly in the western edge of the Hellenic Volcanic Arc. While stable regions demonstrated negligible displacement, areas experiencing subsidence processes necessitate continued vigilance, especially in regions prone to geothermal activity and mass movements.

Comparisons with neighboring regions, such as Methana Peninsula and Poros Island, revealed consistent stability in deformation, reaffirming the regional context of the observed ground displacement patterns. The absence of deformation consistent with volcanic activity on Aegina Island aligned with geological records and limited seismic activity, attributing the observed subsidence processes to settlement phenomena from past volcanic events and regional geothermal activity. In summary, Aegina Island's ongoing subsidence processes underscore the need for continued monitoring and further investigation into the underlying geodynamic mechanisms shaping the island's landscape. Such insights are crucial for informed hazard assessment and mitigation strategies in the region.

Author Contributions: Conceptualization, I.C.-M. and I.P.; methodology, I.-E.K., D.N. and T.G.; software, I.-E.K. and T.G.; validation, I.-E.K., D.N., I.C.-M. and T.G.; formal analysis, I.-E.K.; investigation, I.-E.K.; resources, I.-E.K. and D.N.; data curation, I.-E.K.; writing—original draft preparation, I.-E.K., D.N. and I.C.-M.; writing—review and editing, I.-E.K., D.N., I.C.-M., T.G., S.L. and I.P.; visualization, I.-E.K. and I.C.-M.; supervision, I.C.-M. and I.P.; project administration, I.P.; funding acquisition, I.P. All authors have read and agreed to the published version of the manuscript.

References

1. Fytikas, M.; Innocenti, F.; Kolios, N.; Manetti, P.; Mazzuoli, R. The Plio-Quaternary volcanism of Saronikos area (western part of the active Aegean volcanic arc). *Ann. Geol. Pays Hell.* **1987**, *33*, 3–45.
2. Francalanci, L.; Vougioukalakis, G.E.; Perini, G.; Manetti, P.A. West-East Traverse along the magmatism of the south Aegean volcanic arc in the lights of volcanological, chemical and isotope data. *Dev. Volcanol.* **2005**, *7*, 65–111. [CrossRef]
3. Vougioukalakis, G.E.; Satow, C.G.; Druitt, T.H. Volcanism of the South Aegean Volcanic Arc. *Elements* **2019**, *15*, 159–164. [CrossRef]
4. Drakatos, G.; Karastathis, V.; Makris, J.; Papoulia, J.; Stavrakakis, G. 3D crustal structure in the neotectonic basin of the Gulf of Saronikos (Greece). *Tectonophysics* **2005**, *400*, 55–65. [CrossRef]
5. Papazachos, B.C.; Karakostas, V.G.; Papazachos, C.B.; Scordilis, E.M. The geometry of the Wadati-Benioff zone and lithospheric kinematics in the Hellenic arc. *Tectonophysics* **2000**, *319*, 275–300. [CrossRef]
6. Makris, J.; Papoulia, J.; Drakatos, G. Tectonic deformation and microseismicity of the Saronikos Gulf, Greece. *Bull. Seismol. Soc. Am.* **2004**, *94*, 920–929. [CrossRef]
7. Ganas, A.; Oikonomou, I.A.; Tsimi, C. NOAfaults: A digital database for active faults in Greece. *Bull. Geol. Soc. Greece* **2013**, *47*, 518–530. [CrossRef]
8. Dietrich, V.J.; Gaitanakis, P.; Mercolli, J.; Oberhaensli, R. Geological map of Greece, Aegina island, 1:25,000. *Bull. Geol. Soc. Greece* **1993**, *28*, 555–566.
9. Muller, P.; Kreutzer, H.; Harre, W. Radiometric dating of two extrusives from a Lower Pliocene marine section on Aegina Island, Greece. *Newslett. Stratigr.* **1979**, *8*, 70–78. [CrossRef]
10. Pe-Pipper, G.; Piper, D.J.W.; Reynolds, P.H. Paleomagnetic stratigraphy and radiometric dating of the Pliocene volcanic rocks of Aegina, Greece. *Bull. Volcanol.* **1983**, *46*, 1–7. [CrossRef]
11. Morris, A. Magnetic fabric and palaeomagnetic analyses of the Plio-Quaternary calc-alkaline series of Aegina Island, South Aegean volcanic arc, Greece. *Earth Planet. Sci. Lett.* **2000**, *176*, 91–105. [CrossRef]
12. Keller, J. The major volcanic events in recent eastern Mediterranean volcanism and their bearing on the probem og Santorini ash layers. In Proceedings of the Acta 1st International Scientific Congress on the Volcano of Thera, Athens, Greece, 15–23 September 1969; Kaloyeropoyloy, A., Ed.; Arch Serv Greece: Athens, Greece, 1969; pp. 152–169.
13. Francalanci, L.; Vougioukalakis, G.E.; Fytikas, M. Petrology and volcanology of Kimolos and Polyegos volcanoes within the context of the South Aegean arc, Greece. In *Cenozoic Volcanism in the Mediterranean Area*; Beccaluva, L., Bianchini, G., Wilson, M., Eds.; Special Paper Geological Society of America: Boulder, CO, USA, 2007; Volume 418, pp. 33–65. [CrossRef]
14. Elburg, M.A.; Smet, I. Geochemistry of lavas from Aegina and Poros (Aegean Arc, Greece): Distinguishing upper crustal contamination and source contamination in the Saronic Gulf area. *Lithos* **2020**, *358–359*, 105416. [CrossRef]
15. Vougioukalakis, G.E.; Fytikas, M. Volcanic hazards in the Aegean area, relative risk evaluation, monitoring and present state of the active volcanic centers. *Dev. Volcanol.* **2005**, *7*, 161–183. [CrossRef]
16. Seismological Network of the Institute of Geodynamics. Available online: https://www.gein.noa.gr/en/networks-equipment/seismological-network-of-institute-of-geodynamics/ (accessed on 14 December 2023).
17. Foumelis, M.; Trasatti, E.; Papageorgiou, E.; Stramondo, S.; Parcharidis, I. Monitoring Santorini volcano (Greece) breathing from space. *Geophys. J. Int.* **2013**, *193*, 161–170. [CrossRef]
18. Lagios, E.; Sakkas, V.; Novali, F.; Bellotti, F.; Ferretti, A.; Vlachou, K.; Dietrich, V. SqueeSAR^{TM} and GPS ground deformation monitoring of Santorini Volcano (1992–2012): Tectonic implications. *Tectonophysics* **2013**, *594*, 38–59. [CrossRef]
19. Papageorgiou, E.; Foumelis, M.; Parcharidis, I. Long- and short-term deformation monitoring of Santorini Volcano> Unrest evidence by DInSAR analysis. *IEEE J. Sel. Top. Appl. Earth Obs. Remote Sens.* **2012**, *5*, 1531–1537. [CrossRef]
20. Papageorgiou, E.; Foumelis, M.; Trasatti, E.; Ventura, G.; Raucoules, D.; Mouratidis, A. Multi-sensor SAR geodetic imaging and modelling of Santorini volcano post-unrest response. *Remote Sens.* **2019**, *11*, 259. [CrossRef]
21. Papoutsis, I.; Papanikolau, X.; Floyd, M.; Ji, K.H.; Kontoes, C.; Paradissis, D.; Zacharis, V. Mapping inflaction at Santorini volcano, Greece, using GPS and InSAR. *Geophys. Res. Lett.* **2013**, *40*, 267–272. [CrossRef]
22. Parks, M.M.; Biggs, J.; England, P.; Mather, T.A.; Nomikou, P.; Palamartchouk, K.; Papanikolau, X.; Paradissis, D.; Parson, B.; Pyle, D.M.; et al. Evolution of Santorini Volcano dominated by episodic and rapid fluxes of melt from depth. *Nat. Geosci.* **2012**, *5*, 749–754. [CrossRef]

23. Gatsios, T.; Cigna, F.; Tapete, D.; Sakkas, V.; Pavlou, K.; Parcharidis, I. Copernicus Sentinel-1 MT-InSAR, GNSS and Seismic Monitoring of Deformation Patterns and Trends at the Methana Volcano, Greece. *Appl. Sci.* **2020**, *10*, 6445. [CrossRef]

24. Parcharidis, I.; Lagios, E. Deformation in Nisyros volcano (Greece) using differential radar interferometry. *Bull. Geol. Soc. Greece* **2001**, *34*, 1587. [CrossRef]

25. Lagios, E.; Sakkas, V.; Parcharidis, I.; Dietrich, V. Ground deformation of Nisyros Volcano (Greece) for the period 1995-2002. Results from DInSAR and DGPS observations. *Bull. Volcanol.* **2005**, *68*, 201–214. [CrossRef]

26. Lekkas, E.; Meletlidis, S.; Kyriakopoulos, K.; Manousaki, M.; Mavroulis, S.; Kostaki, E.; Michailidis, A.; Gogou, M.; Mavrouli, M.; Castro-Melgar, I.; et al. The 2021 Cumbre Vieja volcano eruption in La Palma (Canary Islands). *Newsl. Environ. Disaster Cris. Manag. Strateg.* **2021**, *26*. [CrossRef]

27. Ebmeier, S.K.; Andrews, B.J.; Araya, M.C.; Arnold, D.W.D.; Biggs, J.; Cooper, C.; Cottrell, E.; Furtney, M.; Hickey, J.; Jay, J.; et al. Synthesis of global satellite observations of magmatic and volcanic deformation: Implications for volcano monitoring & the lateral extent of magmatic domains. *J. Appl. Volcanol.* **2018**, *7*, 2. [CrossRef]

28. Dzurisin, D. A comprehensive approach to monitoring volcano deformation as a window on the eruption cycle. *Rev. Geophys.* **2003**, *41*, 1001. [CrossRef]

29. Wicks, C.W.; Thatcher, W.; Dzurisin, D.; Svarc, J. Uplift, thermal unrest and magma intrusion at Yellowstone caldera. *Nature* **2006**, *440*, 72–75. [CrossRef] [PubMed]

30. Ghaderpour, E.; Mazzanti, P.; Bozzano, F.; Mugnozza, G.S. Ground deformation monitoring via PS-InSAR time series: An industrial zone in Sacco River Valley, central Italy. *Remote Sens. Appl. Soc. Environ.* **2024**, *34*, 101191. [CrossRef]

31. Orellana, F.; Moreno, M.; Yáñez, G. High-Resolution Deformation Monitoring from DInSAR: Implications for Geohazards and Ground Stability in the Metropolitan Area of Santiago, Chile. *Remote Sens.* **2022**, *14*, 6115. [CrossRef]

32. Berardino, P.; Fornaro, G.; Lanari, R.; Sansoti, E. A new algorithm, for surface deformation monitoring based on small baseline differential SAR Interferograms. *IEEE Trans. Geosci. Remote Sens.* **2002**, *40*, 2375–2383. [CrossRef]

33. Manunta, M.; De Luca, C.; Zinno, I.; Casu, F.; Manzo, M.; Bonano, M.; Fusco, A.; Pepe, A.; Onorato, G.; Berardino, P.; et al. The parallel SBAS approach for Sentinel-1 interferometric wide swath deformation time-series generation: Algorithm description and products quality assessment. *IEEE Trans. Geosci. Remote Sens.* **2019**, *57*, 6259–6281. [CrossRef]

34. Di Traglia, F.; De Luca, C.; Manzo, M.; Nolesini, T.; Casagli, N.; Lanari, R.; Casu, F. Joint exploitation of space-borne and ground-based multitemporal InSAR measurements for volcano monitoring: The Stromboli volcano case study. *Remote Sens. Environ.* **2021**, *260*, 112441. [CrossRef]

35. Ferretti, A. *Satellite InSAR Data—Reservoir Monitoring from Space*, 1st ed.; EAGE: Bunnik, The Netherlands, 2014; pp. 9–100.

36. Singh Virk, A.; Singh, A.; Mittal, S.K. Advanced MT-InSAR Landslide Monitoring: Methods and Trends. *J. Remote Sens. GIS* **2018**, *7*, 1–6. [CrossRef]

37. Yazbeck, J.; Rundle, J.B. A Fusion of Geothermal and InSAR Data with Machine Learning for Enhanced Deformation Forecasting at the Geysers. *Land* **2023**, *12*, 1977. [CrossRef]

38. Guo, H.; Yuan, Y.; Wang, J.; Cui, J.; Zhang, D.; Zhang, R.; Cao, Q.; Li, J.; Dai, W.; Bao, H.; et al. Large-Scale Land Subsidence Monitoring and Prediction Based on SBAS-InSAR Technology with Time-Series Sentinel-1A Satellite Data. *Remote Sens.* **2023**, *15*, 2843. [CrossRef]

39. Li, J.; Yan, Y.; Cai, J. LOS Deformation Correction Method for DInSAR in Mining Areas by Fusing Ground Data without Control Points. *Remote Sens.* **2023**, *15*, 4862. [CrossRef]

40. Poland, M.P.; Zebker, H.A. Volcano geodesy using InSAR in 2020; the past and next decades. *Bull. Volcanol.* **2022**, *84*, 27. [CrossRef]

41. Ezquerro, P.; Bru, G.; Galindo, I.; Montserrat, O.; García-Davalillo, J.C.; Sánchez, N.; Montoya, I.; Palamá, R.; Mateos, R.M.; Pérez-López, R.; et al. Analysis of SAR-derived products to support emergency management during volcanic crisis: La Palma case study. *Remote Sens. Environ.* **2023**, *295*, 113668. [CrossRef]

42. Sakkas, V. Ground deformation modelling of the 2020 M_W 6.9 Samos earthquake (Greece) based on InSAR and GNSS data. *Remote Sens.* **2021**, *13*, 1665. [CrossRef]

43. Beccaro, L.; Tolomei, C.; Gianardi, R.; Sepe, V.; Bisson, M.; Colini, L.; De Ritis, R.; Spinetti, C. Multitemporal and multisensory InSAR analysis for ground displacement field assessment at Ischia volcanic island (Italy). *Remote Sens.* **2021**, *13*, 4253. [CrossRef]

44. Parks, M.; Sigmundsson, F.; Sigurdsson, O.; Hooper, A.; Hreinsdóttir, S.; Ófeigsson, B.; Michalczewska, K. Deformation due to geothermal explotation at Reykjanes, Iceland. *J. Volcanol. Geotherm. Res.* **2020**, *391*, 1064338. [CrossRef]

45. Doke, R.; Kikugawa, G.; Itadera, K. Very local subsidence near the hot spring region in Hakone Volcano, Japan, inferred from InSAR time series analysis of ALOS/PALSAR data. *Remote Sens.* **2020**, *12*, 2842. [CrossRef]

46. Li, M.; Ge, D.; Guo, X.; Zhang, L.; Liu, B.; Wang, Y.; Wu, Q.; Wan, X.; Wang, Y. Mapping and Analyses of Land Subsidence in Hengshui, China, Based on InSAR Observations. *Land* **2023**, *12*, 1684. [CrossRef]

47. Rehman, M.U.; Zhang, Y.; Meng, X.; Su, X.; Catani, F.; Rehman, G.; Yue, D.; Khalid, Z.; Ahmad, S.; Ahmad, I. Analysis of Landslide Movements Using Interferometric Synthetic Aperture Radar: A Case Study in Hunza-Nagar Valley, Pakistan. *Remote Sens.* **2020**, *12*, 2054. [CrossRef]

48. Salepci, N.; Thiel, C. Radar Remote Sensing—Introduction into SAR measurements, Data characteristics & challenges. In Proceedings of the ESA PECS SAR Remote Sensing Course, Bratislava, Slovakia, 17–21 September 2018; Friedrich Schiller University: Jena, Germany, 2018.

49. Lanari, R.; Mora, O.; Manunta, M.; Mallorqui, J.J.; Berardino, P.; Sansosti, E. A small-baseline approach for investigations deformations on full-resolution differential SAR interferograms. *IEEE Trans. Geosci. Remote Sens.* **2004**, *42*, 1377–1386. [CrossRef]
50. Nikaein, T.; Ianninni, L.; Molijn, R.A.; Lopez-Dekker, P. On the value of Sentinel-1 InSAR coherence time-series for vegetation classification. *Remote Sens.* **2021**, *13*, 3300. [CrossRef]
51. Médail, F. Plant biogeography and vegetation patterns of the Mediterranean Islands. *Bot. Rev.* **2022**, *88*, 63–129. [CrossRef]
52. Gkougkoustamos, I.; Krassakis, P.; Kalogeropoulou, G.; Parcharidis, I. Correlation of Ground Deformation Induced by the 6 February 2023 M7.8 and M7.5 Earthquakes in Turkey Inferred by Sentinel-2 and Critical Exposure in Gaziantep and Kahramanmaraş Cities. *GeoHazards* **2023**, *4*, 267–285. [CrossRef]
53. Ka, M.-H.; Shimkin, P.E.; Baskakov, A.I.; Babokin, M.I. A New Single-Pass SAR Interferometry Technique with a Single-Antenna for Terrain Height Measurements. *Remote Sens.* **2019**, *11*, 1070. [CrossRef]
54. Younis, M. Synthetic Aperture Radar (SAR): Principles and Applications. University of Agriculture and Veterinary Medicine. In Proceedings of the 6th ESA Advanced Training Course on Land Remote Sensing, Bucharest, Romania, 14–18 September 2015.
55. Karavias, A. Monitoring Impacts of Climate Change on Surface Subsidence Using SAR Interferometry after the Activation of Karla Lake Reservoir for Water-Consuming Control for Irrigation. Master's Thesis, Harokopio University, Athens, Greece, 2021.
56. Hu, J.; Ge, Q.; Liu, J.; Yang, W.; Du, Z.; He, L. *Theory and Application of Monitoring 3-D Deformation with InSAR*; Science Press: Beijing, China, 2021.
57. Liu, G.; Chen, Q.; Chen, X.; Cai, G. *InSAR Principles and Applications*; Science Press: Beijing, China, 2019.
58. Centre Sismologique Euro-Méditerranéen, Euro-Mediterranean Seismological Centre. Search Earthquakes in the Period 1 January 2016 to 31 May 2023. Available online: https://www.emsc-csem.org/Earthquake_information/ (accessed on 20 March 2024).
59. Matsuda, J.; Senoh, K.; Maruoka, T.; Sato, H.; Mitropoulos, P. K-Ar ages of the Aegean volcanic rocks and their implications for the arc-trench system. *Geochem. J.* **1999**, *33*, 369–377. [CrossRef]